ACS Photonics

pubs.acs.org/journal/apchd5

Article

Rapid Imaging of Pulsed Terahertz Radiation with Spatial Light Modulators and Neural Networks

Rayko Ivanov Stantchev,[‡] Kaidi Li,[‡] and Emma Pickwell-MacPherson*

Cite This: https://doi.org/10.1021/acsphotonics.1c00634

Read Online

ACCESS | Metrics & More | Article Recommendations | Supporting Information

ABSTRACT: We report the first use of a convolutional neural network for terahertz (THz) imaging combined with a single-pixel camera to achieve high quality hyperspectral THz imaging 10× faster than the current commercial systems, with faster potential only limited by noise. Imaging with a spatial light modulator (SLM) relies on projecting a set of spatial patterns onto an object and recording the transmission with a single-pixel detector, and an optical delay unit (ODU) is used to obtain the terahertz time-of-flight information. A key breakthrough in this work is to synchronize the equipment to not need any time to instruct the ODU to move while projecting the patterns.

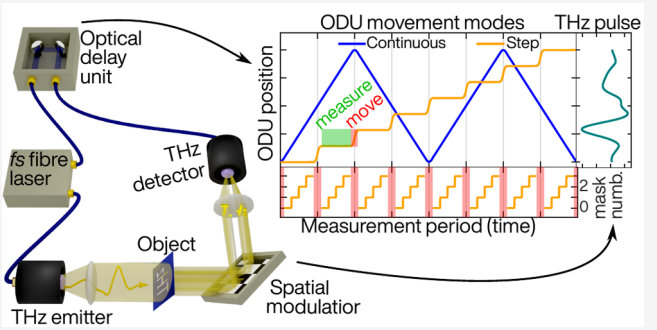

KEYWORDS: *terahertz imaging, single-pixel detectors, spatial light modulation, time-domain spectroscopy, neural networks*

Terahertz (THz) time-domain spectroscopy (TDS) has generated a great body of research.[1] TDS systems measure the amplitude and phase information of a THz wave, thereby allowing easy calculation of the THz complex refractive index, giving insight into the charge-carrier dynamics of semiconductors[2] and crystal quality of perovskites[3] for example. Furthermore, the time-of-flight information can be used to create a 3D image showing the subsurface layers of optically opaque materials.[4] The nonionizing THz photon energies also hold potential for cancer diagnosis.[5] Despite these capabilities, imaging with time-resolved THz spectrometers is not widely used outside of laboratory settings.

Current commercial THz-TDS imaging systems work by raster scanning either the object or the emitter−detector pair, resulting in a slow acquisition of around 20−30 data pixels per second due to mechanical movement. This slow imaging rate is unappealing to the semiconductor industry and renders hospital use unpractical. Raster scanning mechanisms are typically employed as detector arrays that can measure the amplitude and phase of a THz wave that are not readily available. Although using microbolometer arrays in conjunction with digital holography can achieve coherent imaging at a single frequency,[6,7] they lack the subpicosecond temporal resolution that THz-TDS offers. Using an optical camera to map the THz fields in an electro-optic crystal[8] is a viable alternative; this, however, requires a regeneratively amplified Ti:sapphire laser, which severely reduces the pulse repetition rate (slower acquisition) and increases the system size and cost.

Using a single-pixel detector and a spatial light modulator has recently become an alternative imaging method to overcome the drawbacks of the aforementioned approaches.[9] Such single-pixel cameras are typically slower than ones based on detector arrays, but they are more robust and accessible for frequencies outside the visible-light regime. This makes them highly suited for THz imaging. Single-pixel THz cameras do exist[10,11] and they have been used for inspection of circuits hidden behind semiconductors,[12] for example, as well as for near-field THz imaging of solid state systems[13−16] and biological samples as well.[17] There have also been studies showing 2D tomographic imaging[18] and potential for standoff applications.[19] Previously, we showed that a THz video can be obtained and displayed in real-time with a single-pixel THz camera.[20] However, hitherto there has not been a single study on how to best use a SLM for time-resolved THz imaging.

Here, we consider and optimize the synchronization between a spatial THz modulator and an optical delay unit (ODU), commonly used in THz-TDSs to acquire time-of-flight information. We show how to eradicate the time needed to instruct the ODU to move while simultaneously projecting our masks. This removes a dead waiting time that would otherwise impede any further reductions in acquisition time, with the fundamental limit imposed by the SLM switch-rate only. We demonstrate temporal undersampling procedures, reducing measurement times by 70% and a neural network is

Received: April 26, 2021

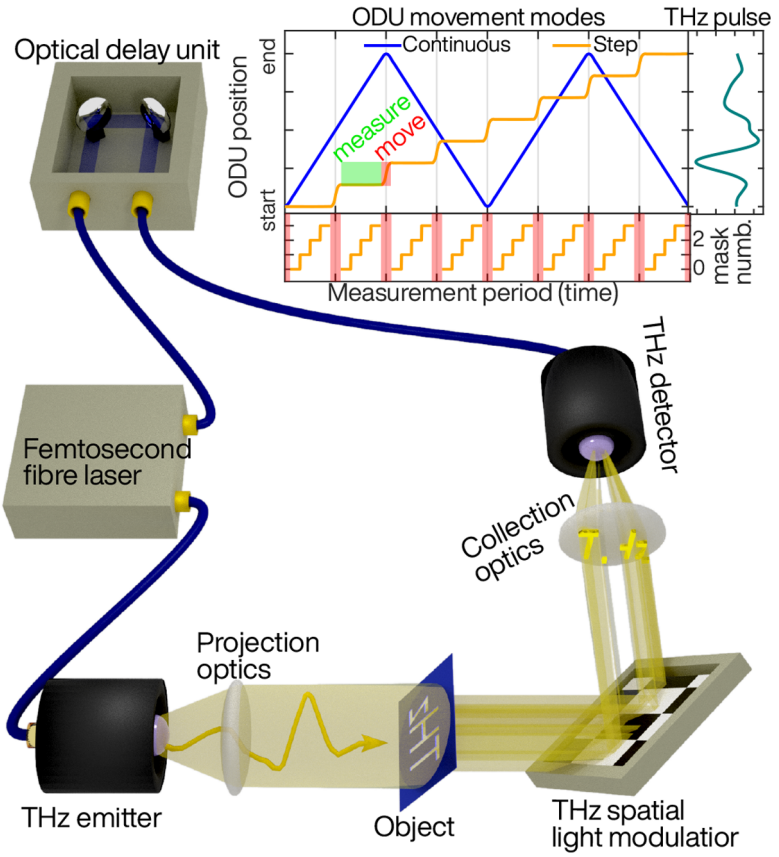

Figure 1. Illustration of the experimental setup: A femtosecond fiber laser (100 fs, 1550 nm) sends a pulse to a photoconductive THz emitter. The train of THz pulses pass through an object, then a spatial THz modulator (see ref 20 for details), and finally, all the light is measured with a photoconductive detector. There is an optical delay unit (ODU) between the THz receiver and fiber laser that changes the arrival times between the optical detection pulses and the THz pulses, thus, allowing the measurement of the THz field strength at different temporal points. Inset: Depiction of the two ODU movement modes. The bottom graph depicts how the masks are displayed on the SLM during each measurement stage of the step-mode, with the red areas showing the time waited for the ODU to move.

built to improve the quality of our THz data allowing five times faster acquisition rates to be used. Ultimately, in under 3 s we obtain high-quality THz images with 32 × 32 data pixels over a 10 ps time window with 100 time frames. This is 10× faster than the state-of-the-art.

Figure 1 illustrates the experimental setup. A femtosecond fiber laser powers a photoconductive emitter to generate a beam of THz pulses, which then propagate through an object onto a spatial THz light modulator and are finally detected by a photoconductive detector. An optical delay line controls the temporal position at which we are sampling the THz field. The system is a MENLO K15 fiber-based THz-TDS with an 80 MHz pulse repetition rate, where the (100 fs, 1500 nm) pulses power a pair of photoconductive antennas that use low temperature grown GaAs with subpicosecond carrier lifetimes as the semiconductor, and we use a NI USB-6351 DAQ card with a 250 kHz acquisition rate to readout the detected signal. For our spatial THz modulator, we photoexcite silicon with a spatially patterned 450 nm continuous-wave laser.[20] Note the silicon used here has carrier lifetimes of 65 μs, as opposed to 250 μs in our previous work,[20] to achieve quicker switch rates. Thus, our physical masks are effectively binary, having values of [1, 0] for the masks and values of [1, −1] for the differential masks (signal from the positive mask minus the signal from the complementary inverse mask).

Obtaining an image with a spatial light modulator (SLM) works by projecting a set of masking patterns onto an object and using a single-element detector to record the resulting transmission (or reflection) of an object for each pattern. Since the recorded signals are correlations between the object and the masking patterns, computers can reconstruct an image of the object via matrix inversion or other minimization algorithms.[9] Therefore, a simple way of obtaining a THz image that contains temporal data, that is, a 3D image with one temporal and two spatial dimensions, which can be used in hyperspectral THz analysis,[1,2] is the following: project the set of masking patterns needed to recover a 2D image, then move the delay line to the next temporal point, and project the set of masking patterns again. Repeat this until we can obtain an individual 2D image at each temporal point of interest. We call this ODU movement mode "step-mode", and it is illustrated in yellow in the inset of Figure 1. While very simple and easy to setup, this mode suffers from one major drawback, namely, instructing the ODU when to move and waiting for it to arrive at the next temporal point adds dead time where we are not measuring. An alternative movement mode is for the ODU to continuously oscillate backward and forward in a triangle-wave manner between the start and end temporal points, while we simultaneously project our set of masking patterns a number of times. This ODU movement mode we call "continuous-mode", and it is illustrated by the blue line in the inset of Figure 1.

https://doi.org/10.1021/acsphotonics.1c00634
ACS Photonics XXXX, XXX, XXX−XXX

Step-mode has a simple reconstruction algorithm for our 3D images; since we project our mask set at the same temporal point and move only after finishing the projection, we can easily recover a 2D image at this and every other temporal point. However, in continuous-mode the masks are projected at different temporal points, hence, the challenge is to recover a 2D image at time t when some masks were projected at t and others at $t + \delta t$. If δt is infinitesimally small, then we have no problem. However, we encounter a problem once δt is large enough for us to consider t and $t + \delta t$ to be different temporal points on the THz waveform, that is, they have distinct values on the detector. This is related to the temporal resolution of the detector, which is 100 fs, as set by the optical pulses from our MENLO K15 system that uses a low-temperature grown GaAs photoconductive detector with subpicosecond lifetimes. However, in practice, we can observe a difference between two temporal points spaced by 50 fs at the maximum and minimum of the gradient of the THz pulse, hence, we expect to have image reconstruction problems if $\delta t > 50$ fs. In our experiment, this δt value is set by the rate at which we change our spatial masks and the oscillation frequency of our ODU.

The simplest scenario is for the ODU to perform half a cycle during the measurement period and the spatial masks to be changed such that the temporal distance between the first and last mask, of the mask set needed to recover a 2D image, is less than 50 fs. Another simple scenario is to change the SLM pattern every time the ODU has completed half a cycle, that is, record the THz pulse for mask one then change to mask two. While this circumvents the problem with δt, these two scenarios suffer from one major drawback. Namely, temporal-undersampling is impossible, and we want to minimize the total measurement time. As per the Fourier analysis of signals, sampling at temporal-intervals shorter than our detector response will give us no new information other than smoother looking data. Our THz detector has a temporal-resolution of 100 fs due to the width of the pulses powering it, hence, for temporal undersampling we need to have fewer sampling points than the total temporal-distance divided by 100 fs, a quantity we call N. For us, this means that we need to project the whole 2D-mask set fewer times than this number and obtain a set of 2D images to construct our 3D-THz image without causing significant degradation.

The step-mode has an easy undersampling implementation.[21] THz pulses are sparse in that the energy is temporally concentrated around a single point and there are large intervals with near-zero values. Therefore, we only need to concentrate taking 2D-images where most of the energy is and ignore other areas. This can be accomplished via two-stage adaptive sampling; first we measure a coarsely distributed sampling, every 1 ps for example, then second add more sampling points around where we have measured the largest THz amplitudes, as we believe most of the THz pulse energy to be located around here. Reference[21] shows this can reduce the number of measurement points needed by half and still get very good results when performing spectroscopic THz analysis.

Continuous-mode does have an equivalent adaptive sampling technique, which would be to reduce the ODU movement speed where the pulse is located. Unfortunately, our ODU can only oscillate in a triangle-wave manner, as shown in the inset of Figure 1, hence, we can not experimentally analyze this idea and only discuss it in Supporting Information, section 1. The simplest way of discussing undersampling in the continuous-mode is to think of the projection of patterns as taking the form of a stepped saw-wave and considering the frequency of this saw-wave, f_s, and the frequency of ODU triangle-wave, f_t. Our task is to find the optimum ratio between these frequencies f_s/f_t with the constraint that we want f_s or f_t to perform fewer cycles than N or $N/2$, respectively, during our measurement period. It is important that f_s and f_t are not multiples of each other. The reason for this can be seen in the inset of Figure 1 where $f_s = 4f_t$. If we look at the first and fifth times mask 0 is projected, we find that both projections were at the starting point of the ODU movement range. This means that, during the second triangle-wave cycle, we did not obtain new temporal information, but only better averaging for mask 0 and, consequently, every other mask. Therefore, it is best if f_s and f_t are both prime numbers and this is discussed in detail in Supporting Information, section 1. Note, our hardware lacks the precision to thoroughly study when f_t is large, thus, this is only discussed in the Supporting Information. We define the temporal sampling ratio, T_r, as the number of cycles f_s has performed during the whole measurement, divided by N. The temporal undersampling requirement means that $\delta t > 100$ fs, hence, we can expect reconstruction problems for the 2D images, especially around the maxima and minima of the THz pulse gradient.

Figure 2a shows a THz pulse and the detected values from binary Hadamard masks with values of $[1, 0]$, centered around 4.25 ps as taken with the ODU in the continuous mode. The inset shows the $[1, 0]$ mask measurements compared against the measurements from the differential $[1, -1]$ masks taken at the same temporal positions with the coefficient number along the x-axis. Figure 2b−p shows 2D THz images at different temporal times, as recovered from $[1, 0]$ and $[1, -1]$ Hadamard masks in the top and middle rows, respectively, with the ODU moving in the continuous mode with $T_r = 0.6$. The ground truth images (bottom row) were taken using the same $[1, -1]$ Hadamard masks, but the ODU was moving in step-mode with $T_r = 1$. We choose the step-mode for the ground truth because we want to be certain that the continuous imaging mode does not introduce any temporal errors or artifacts. For all the 32×32 images, we measured the 256 coefficients with the lowest sequency, as defined by the 2D Hadamard transformation (see Supporting Information, section 3, for details), since Hadamard masks are easy to implement with our THz-SLM.[20] This spatial undersampling is performed for the ground truths as well since spatial undersampling of images has been extensively studied,[9] and this work concerns itself with how the temporal nature of THz-TDS measurements affects single-pixel imaging.

The signals from the $[1, 0]$ mask in Figure 2a are a complete set of the 256 coefficients we use to reconstruct a 2D image, with all of them measured in the temporal interval of 4 and 4.5 ps. It can be seen that the masks around 4 ps have lower amplitudes than those around 4.5 ps, in line with the slope of the THz pulse. Comparing the signals from the $[1, -1]$ and $[1, 0]$ masks in the inset, it can be seen that most of the $[1, -1]$ signals have very little energy, as expected from Hadamard transforms of images. By contrast, the $[1, 0]$ signals have large curve-shaped artifacts caused by the THz pulse gradient. Since the signals for the $[1, -1]$ masks were obtained by projecting a mask followed by its inverse and taking the difference, this procedure has effectively subtracted out the THz pulse gradient and removed the errors it causes. In Figure 2b−p, we can see that the images from $[1, 0]$ masks (top row) have severe artifacts, whereas the $[1, -1]$ images (middle row) do

https://doi.org/10.1021/acsphotonics.1c00634
ACS Photonics XXXX, XXX, XXX−XXX

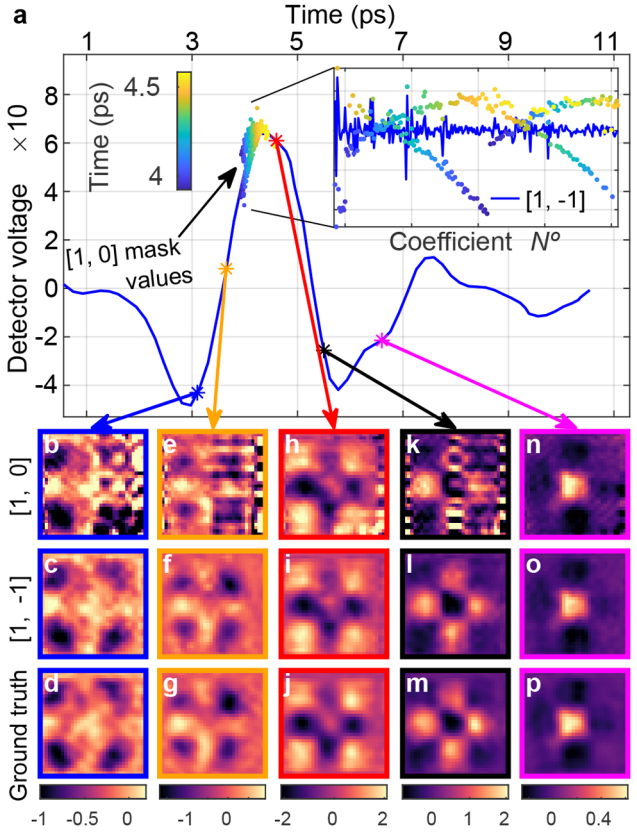

Figure 2. (a) Detected signals from [1, 0] Hadamard masks centered around 4.2 ps shown alongside a THz pulse (blue line) for comparison. Inset: the same [1, 0] mask signals plotted against their Hadamard coefficient number along the *x*-axis. The solid blue line shows the same coefficients as measured by [1, −1] masks. Note the [1, 0] was shifted by subtracting the mean of the ensemble. (b−p) 32 × 32 THz images at individual temporal points along the columns and the top, middle, and bottom rows being images taken with [1, −1] and [1, 0] masks and ground truth, respectively. The image temporal times are shown by arrows coming from (a). Field of view is 1 × 1 cm, with acquisition times being 17.1, 34.2, and 47.2 s for a single 3D image in the [1, 0], [1, −1], and ground truth images, respectively. Note the ground truth is an average of 18 measurements.

not when compared to the ground truth images (bottom row). It should be noted that a different measurement matrix would result in different image artifacts. Framing the problem as a minimization problem of the form $y = Ax$ is infeasible, as even our modest 32 × 32 × 100 images would be a computationally heavy problem. Therefore, we choose a 3D image reconstruction procedure that uses interpolation to temporally align all the measurements, with the details shown in Supporting Information, section 4.

Using a differential measurement of a [1, 0] mask and its inverse to obtain a [1, −1] sampling matrix usually doubles the number of measurements needed. However, single-pixel Fourier imaging can obtain the equivalent [1, −1] matrix via a three-shift method increasing the number of measurements by 3/2.[22] For this reason, we demonstrate the implementation of Fourier masks with our THz-SLM in Supporting Information, section 3 and use them in the following parts of this work. Noise in the measurement and artifacts from implementing temporal undersampling will heavily influence the acquisition rate, provided we are not near the limits of our equipment. In our previous work we showed that our modulator can reach up to a 20 kHz switch rate,[20] however, our signal-to-noise was not sufficiently high to acquire images of viewable quality at that switch rate, as the data needed to be averaged 16 times. Therefore, noise limits our acquisition speeds and not equipment or any physical phenomena, thus, to improve image quality when imaging at high SLM switch-rates we explore image denoising algorithms in Supporting Information, S5. We find that a neural network is able to post-process our raw images in real-time as well as having the largest reduction in noise and artifacts from the measurement. The second best improvement in image quality was by Wiener filtering, which was also able to display the denoised images in real-time. Other methods studied were total variational minimization and wavelet denoising, both of which had similar improvements in image quality, although neither were able to process the images fast enough for real-time display. Thus, our results from Supporting Information, S5 indicate that, for real-time display applications, deep learning methods should be used if training data is available; otherwise, Wiener filtering will give a very good result. The data we gathered and our processing scripts can be downloaded: see the data availability statement.

The structure similarity index measure (SSIM) is a common quantity when studying the quality of images that are affected by noise and compression. Figure 3 shows how the SSIM of

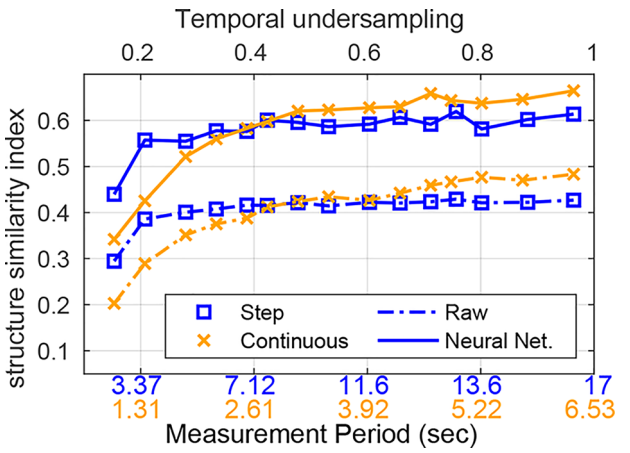

Figure 3. Structure similarity index as a function of temporal undersampling of 3D-THz images, with the dash-dotted (solid) line showing the SSIM of the raw (neural network processed) images. The bottom axis shows the total time the measurement took, with top (bottom) numbers being for the step (continuous) ODU mode. SLM switch rate was 5 kHz and 294 Fourier-based masks sampled each 2D image.

our 3D images behaves when we perform temporal undersampling with the THz data shown in Supporting Information, video 1. The neural network has improved the SSIM by around 0.2, while keeping the same trend with regard to T_r. Note that we get an SSIM around 0.6 when the SLM switch-rate is 5× slower, as shown in Supporting Information, Figure 16. This in effect means that the network has removed measurement noise; however, the artifacts from temporal-undersampling are still present. This is because the measurement noise can be readily identified in the 2D-images, whereas the artifacts from temporal-undersampling can only be seen in the full 3D-data (made up of 2D-image stacks). Our network processes each individual 2D image by itself only to show that neural networks

https://doi.org/10.1021/acsphotonics.1c00634
ACS Photonics XXXX, XXX, XXX−XXX

can be used to improve the quality of 3D THz data. Moreover, building a network that can process data at multiple undersampling ratios is unfeasible as it would be much more efficient to create a network that removes artifacts at a single undersampling amount, for example, at T_r = 0.2 or lower. Further, the noise artifacts from the continuous and step modes are different and thus are likely to require different networks, likewise if extracting spectral information[3] or thicknesses from THz pulse delays.[4]

Figure 3 shows that the SSIM of the step-mode has a superior performance once the T_r becomes smaller. This is expected, as it employs a two-stage adaptive sampling algorithm[21] that concentrates measurements where the THz waveform has large amplitudes, whereas in continuous-mode, our hardware can not implement the equivalent motion. Therefore, it is inappropriate to do an exact comparison. Nevertheless, we can see that, for $T_r > 0.5$, the SSIM for both step and continuous modes is of similar values, indicating that the continuous-mode does not introduce any additional errors or temporal artifacts when compared to the step-mode; therefore, the step-mode does not need to be used other than to check if all the equipment was synchronized correctly in the continuous-mode. This is significant, as the continuous-mode offers substantially quicker acquisition rates. In the inset of Figure 1, we can see that the total measurement time for the step-mode is going to be the time needed to acquire a single 2D-image and then move the ODU multiplied by the number of temporal-points we want to measure. The time needed to acquire a 2D-image is determined by the number of spatial masks and the SLM switch-rate, and in Figure 3 we use 294 masks switched at a 5 kHz rate; thus, we need 58.8 ms to acquire a 2D-image. The time needed by our ODU to move is about 75 ms, with 25 ms due to software synchronization and 50 ms due to acceleration and deceleration of the ODU. This creates a bottleneck in reducing the total acquisition time, since reducing the time needed to acquire a 2D-image by a quicker SLM or by projecting fewer masks would not result in any meaningful improvement in the overall acquisition rate. This is why the continuous ODU mode is around 3× quicker than the step-mode for the same T_r, we are using more time waiting for the ODU to move than measuring. The significance of this for future research is that developing quicker THz-SLMs for continuous-mode will give meaningful improvements in the acquisition rate, assuming sufficient signal levels, whereas for step-mode there will be no meaningful improvements.

In terms of the absolute limits of our system, we use a photoconductive antenna detector with subpicosecond carrier lifetimes and the laser system has an 80 MHz pulse repetition rate. Due to these short carrier lifetimes, the pulse repetition rate will set the ultimate acquisition rate of fiber based THz-TDS systems such as ours. However, a more realistic limit would be closer to 80 kHz because it is likely that 1000 pulses are needed to be measured for a single mask value to average out laser noise. Additionally, the future antennas used for this type of imaging should be those developed for emitting a beam, whereas the emitter detector pair we used was optimized for focusing the radiation into a spot for raster scanning.

It should be noted that we originally tried to use the CIFAR-10 image data set to simulate our experiment and train the neural network. However, this gave suboptimal results due to the following: first, visible light images have very different physical resolution to our THz radiation, leading the network to create fictitious objects; second, these images are intensity based and are scaled between 0 and 1, whereas our THz images have positive and negative values, hence, the network struggles to preserve the energy in each THz image making spectroscopic analysis impossible; third, the noise in our THz system is difficult to model; any noise in the femtosecond fiber laser manifests itself as source and detector noise simultaneously in a nonlinear manner, and this is in addition to electrical noise. We can not measure the laser noise simultaneously to our THz signals and thus we can only make guesses into our THz system's noise. Thus, without an accurate noise model the resulting network would sometimes enhance features which were actually due to experimental noise. This is why we had to build our own data set suitable for our THz-TDS imaging system. A further note is that since THz radiation has potential uses in cancer diagnosis,[5] clinical trials will be performed and the raw data from these trials will be sufficient to build a database of THz images that could be used as training data for neural networks. This would spare THz researchers from the effort of building a database for training, although for applications like semiconductor/electronics quality control solving the aforementioned problems and using an existing image database might prove to be a more efficient solution.

This work optimizes single-pixel THz cameras for time-domain measurements. We completely remove the time usually needed to instruct the ODU to move forward, which means only the system noise and THz-SLM switch rate limit the acquisition rate. We demonstrate that the THz waveform gradients need to be subtracted out from the measurement, which we do by using a differential mask measurement (although using a second detector should achieve the same result). We use a neural network to improve our images and show it is possible to acquire a 32 × 32 THz image over a 10 ps temporal-interval, with 100 frames in under 3 s, about 10× faster than commercial raster-scanning based THz-TDS imaging systems. The most interesting aspect of this work is that there is no inherently expensive equipment involved, and the potential of achieving faster acquisition is restricted by noise and not equipment capabilities. Given the large range of possible applications of single-pixel THz cameras,[12,13,15−19] future work will need to focus on optical designs for more specific applications, such as skin imaging or semiconductor quality control.

■ ASSOCIATED CONTENT

Supporting Information

Supporting Information is available free of charge via the Internet at . The Supporting Information is available free of charge at https://pubs.acs.org/doi/10.1021/acsphotonics.1c00634.

List of materials: S1, Adaptive sampling distribution in continuous ODU mode; S2, ODU speed and SLM switch rate relationship; S3, Single-pixel imaging; S4, Raw signals and processing; S5, Convolutional neural network (PDF)

Video 1 (AVI)

■ AUTHOR INFORMATION

Corresponding Author

Emma Pickwell-MacPherson − *Chinese University of Hong Kong, Electronic Engineering, Hong Kong, SAR, China;*

https://doi.org/10.1021/acsphotonics.1c00634
ACS Photonics XXXX, XXX, XXX−XXX

University of Warwick, Physics Department, Coventry CV4 7AL, United Kingdom; orcid.org/0000-0001-6062-5959; Email: e.macpherson@warwick.ac.uk

Authors

Rayko Ivanov Stantchev − *Chinese University of Hong Kong, Electronic Engineering, Hong Kong, SAR, China;* orcid.org/0000-0002-0523-7619

Kaidi Li − *Chinese University of Hong Kong, Electronic Engineering, Hong Kong, SAR, China*

Complete contact information is available at: https://pubs.acs.org/10.1021/acsphotonics.1c00634

Author Contributions

‡R.I.S. and K.L. contributed equally to this work. R.I.S., K.L., and E.P.-M. conceived the idea. R.I.S. created the experimental setup and programmed all equipment. K.L. designed the neural network. R.I.S. and K.L. performed the experiments and data analysis. R.I.S. wrote the manuscript, and all others provided editorial input.

Notes

The authors declare no competing financial interest.

DATA AVAILABILITY: All the training data and scripts (MATLAB for raw data processing and Python for network training) needed to reproduce the results of this work can be found on https://doi.org/10.6084/m9.figshare.14236766.

■ ACKNOWLEDGMENTS

This work was partially supported by the Research Grants Council of Hong Kong (Project Numbers 14206717, 14201415), The Hong Kong Innovation and Technology Fund (Project Number ITS/371/16), The Engineering and Physical Sciences Research Council (Grant Number EP/S021442/1), and the Royal Society Wolfson Merit Award (EPM).

■ REFERENCES

(1) Dexheimer, S. L. *Terahertz Spectroscopy: Principles and Applications*, 1st ed.; CRC Press: Boca Raton, FL, 2008.

(2) Ulbricht, R.; et al. Carrier dynamics in semiconductors studied with time-resolved terahertz spectroscopy. *Rev. Mod. Phys.* **2011**, *83*, 543−586.

(3) Sun, Q.; Liu, X.; Cao, J.; Stantchev, R. I.; Zhou, Y.; Chen, X.; Parrott, E. P. J.; Lloyd-Hughes, J.; Zhao, N.; Pickwell-MacPherson, E. Highly Sensitive Terahertz Thin-Film Total Internal Reflection Spectroscopy Reveals in Situ Photoinduced Structural Changes in Methylammonium Lead Halide Perovskites. *J. Phys. Chem. C* **2018**, *122*, 17552−17558.

(4) Dong, J.; et al. Terahertz frequency-wavelet domain deconvolution for stratigraphic and subsurface investigation of art painting. *Opt. Express* **2016**, *24*, 26972−26985.

(5) Cheon, H.; Yang, H.-J.; Son, J.-H. Toward Clinical Cancer Imaging Using Terahertz Spectroscopy. *IEEE J. Sel. Top. Quantum Electron.* **2017**, *23*, 1−9.

(6) Locatelli, M.; et al. Real-time terahertz digital holography with a quantum cascade laser. *Sci. Rep.* **2015**, *5*, 13566.

(7) Yamagiwa, M.; et al. Real-Time Amplitude and Phase Imaging of Optically Opaque Objects by Combining Full-Field Off-Axis Terahertz Digital Holography with Angular Spectrum Reconstruction. *J. Infrared, Millimeter, Terahertz Waves* **2018**, *39*, 561−572.

(8) Usami, M.; et al. Development of a THz spectroscopic imaging system. *Phys. Med. Biol.* **2002**, *47*, 3749−3753.

(9) Gibson, G. M.; et al. Single-pixel imaging 12 years on: a review. *Opt. Express* **2020**, *28*, 28190.

(10) Watts, C. M.; et al. Terahertz compressive imaging with metamaterial spatial light modulators. *Nat. Photonics* **2014**, *8*, 605−609.

(11) Shrekenhamer, D.; et al. Terahertz single pixel imaging with an optically controlled dynamic spatial light modulator. *Opt. Express* **2013**, *21*, 12507.

(12) Stantchev, R. I.; Sun, B.; Hornett, S. M.; Hobson, P. A.; Gibson, G. M.; Padgett, M. J.; Hendry, E. Noninvasive, near-field terahertz imaging of hidden objects using a single-pixel detector. *Sci. advances* **2016**, *2*, e1600190.

(13) Chen, S.-C.; et al. Terahertz wave near-field compressive imaging with a spatial resolution of over $\lambda/100$. *Opt. Lett.* **2019**, *44*, 21−24.

(14) Chen, S.-C.; Feng, Z.; Li, J.; Tan, W.; Du, L.-H.; Cai, J.; Ma, Y.; He, K.; Ding, H.; Zhai, Z.-H.; Li, Z.-R.; Qiu, C.-W.; Zhang, X.-C.; Zhu, L.-G. Ghost spintronic THz-emitter-array microscope. *Light: Sci. Appl.* **2020**, *9*, na.

(15) Stantchev, R. I.; et al. Compressed sensing with near-field THz radiation. *Optica* **2017**, *4*, 989.

(16) Hornett, S. M.; Stantchev, R. I.; Vardaki, M. Z.; Beckerleg, C.; Hendry, E. Subwavelength Terahertz Imaging of Graphene Photoconductivity. *Nano Lett.* **2016**, *16*, 7019.

(17) Barr, L. E.; et al. Super-resolution imaging for sub-IR frequencies based on total internal reflection. *Optica* **2021**, *8*, 88.

(18) Mohr, T.; Herdt, A.; Elsasser, W. 2D tomographic terahertz imaging using a single pixel detector. *Opt. Express* **2018**, *26*, 3353.

(19) Augustin, S.; et al. Terahertz Dynamic Aperture Imaging at Standoff Distances Using a Compressed Sensing Protocol. *IEEE Trans. Terahertz Sci. Technol.* **2019**, *9*, 364−372.

(20) Stantchev, R. I.; et al. Real-time terahertz imaging with a single-pixel detector. *Nat. Commun.* **2020**, *11*, 1−8.

(21) He, Y.; et al. Adaptive Sampling for Terahertz Time-Domain Spectroscopy and Imaging. *IEEE Trans. Terahertz Sci. Technol.* **2017**, *7*, 118−123.

(22) Zhang, Z.; et al. Hadamard single-pixel imaging versus Fourier single-pixel imaging. *Opt. Express* **2017**, *25*, 19619−19639.